An investigation on the vibrations of laminated shells under aeroacoustic loads using a WFE approach

F Errico, F Franco, Mohamed Ichchou, S de Rosa, G. Petrone

An investigation on the vibrations of laminated shells under aeroacoustic loads using a WFE approach

F. Errico[1,2], F. Franco[2], M. Ichchou[1], S. De Rosa[2] and G. Petrone[2]

[1]*LTDS, Laboratoire de Tribologie et Dynamique des Systems, Ecole Centrale de Lyon, 36 Avenue Guy de Collongue, 69134 Écully, France*
[2]*Pasta-Lab, Laboratory for promoting experiences in aeronautical structures and acoustics, Dipartimento di Ingegneria Industriale, Universitá degli Studi di Napoli Federico II, Via Claudio 21, 80125 Napoli, Italy*

(Received September 5th, 2018, Revised March 25th, 2019, Accepted April 29th, 2019)

Abstract. The present work investigates the effect on the flow-induced vibrations of the lay-up sequence of composite laminated axisymmetric structures, using an hybrid approach based on a wave finite element and a transfer matrix method. The structural vibrations, under deterministic distributed pressure loads, diffuse acoustic field and turbulent boundary layer excitations, are analysed and compared. A multi-scale approach is used for the dynamic analysis of finite structures, using an elementary periodic subsystem. Different flow regimes and shell curvatures are analysed and the computational efficiency is also discussed.

Keywords: wave finite element method; flow-induced vibrations; wave propagation; boundary layer excitation

1. Introduction

In the transport industry it is not rare to meet excessive structural vibrations due to random aeroacoustic excitations acting on the structure's surface by means of the pressure fluctuations. While structure-borne acoustic radiation might impact on the comfort of the transport means, the excessive vibrations might lead to undesired flow-induced fatigue problems [Kolaini et al. (2018), Vaquer-Araujo et al. (2018), Mehta (2018)]. This issue is even more evident with sandwich and laminated composite structures, extensively used in modern aerospace as well as in the automotive, naval and civil industry, because they can provide lighter and stronger structures than most metal alloys. At the same time, high computational costs arise, from the point of view of the numerical simulations, when complex sandwich panels are analysed using classical models as, for example, the finite element method (FEM).

The vibrational response of fluid loaded axisymmetric structures can be estimated once data on the distributed pressure distributions are available. While numerical methods can

*Corresponding author, Fabrizio Errico, E-mail: fabrizio.errico@ec-lyon.fr

give accurate case-sensitive surface pressures, simplified semi-empirical models for the wall pressure fields (WPF), and their correlation functions, are present in the literature, for a large variety of excitation models.

The characterisation of the turbulent boundary layer wall pressure fluctuations has first been carried out experimentally by Corcos [Corcos et al. (1963)]. The Corcos model assumes the separation of variables and and exponential dependency versus frequency, for the cross spectral density of the pressure fluctuations, on the distances among points. This model is one of the simplest and most used in literature. To improve the accuracy of the Corcos model in specific wavenumber domains (i.e. the sub-convective domain), Efimtsov et al. (1982) and Ffowcs Williams et al. (1982) proposed a model which is somewhat correlated to the Corcos one, while Smol'yakov et al. (1991) and Chase et al. (1980) proposed formulations with a stream-wise and cross-wise correlation for the pressure fluctuations.

The predictive methodologies available in literature are mainly modal-based and mainly connected to flat panels [Elishakoff et al. (1983), Ichchou et al. (2009), Ciappi et al. (2012), De Rosa et al. (2008a), Franco et al. (2013), Yang et al. (2017)]. Some applications to curved shells have been presented by Birgersson et al. (2004), while some measurements and analyses on full-scale fuselages have also been presented in the literature by Bhat (1971) and Wilby et al. (1972).

Since the computational cost associated to finite element calculations might be excessive, especially under distributed random pressure loads, the convective load can be simulated through a purely coherent or incoherent equivalent load depending on the frequency range of analysis [Franco et al. (2013)]. For example, at high-frequencies, an equivalent rain-on-the-roof excitation can be used in this frequency regime, giving advantages in the calculation of the joint acceptance integrals [Lyon et al. (1995), Ichchou et al. (2009)]. Hybrid SEA/FE methods are also present in the literature, to deal with the medium-high frequencies [Troclet et al. (2009)]. However, since most of these techniques, present in the literature, are limited in terms of accuracy and the computational speed in specific frequency ranges, especially in the medium one, a strong interest is placed on methods to overcome and/or extend these limits [Errico et al. (2018b)]. This paper proposes an hybrid wave based methodology, suitable also for axisymmetric structures.

While in the literature the influence of the lay-up sequence is mainly studied for static and buckling analysis, only a few works investigate the effect of the lamination with a specific vibro-acoustic target, as done by Christen et al. (2016). Here, the effect of the stacking sequence is studied on cylindrical structures under distributed pressure loads, for fixed frequencies, and under turbulent boundary layer excitation.

The work is structured as follows: Section 2 presents a literature survey; Section 3 presents the numerical methodology used for axial-symmetric structures; Section 4 presents a validation of the approach for a large cylindrical shell under a propeller-like deterministic pressure distribution and a tapered axisymmetric structure under a diffuse acoustic field excitation; Section 5 presents a study on cylinders of different radius for various stacking sequences under a turbulent boundary layer excitation.

2. Literature Background

2.1 Analytic Solution

The analytic approach can be developed only for a flat rectangular panel simply-supported along the edges. The approach, developed in [Elishakoff et al. (1983)], is further analysed in [De Rosa et al. (2008a), Franco et al. (2013), De Rosa et al. (2008b)]. The final equation is here shown for sake of completeness, [De Rosa et al. (2008b)]:

$$\mathbf{S}_{ww}(x_a, y_a, \omega) = \sum_j \sum_n \Big[\frac{\Psi_j(x_a, y_a)\Psi_n(x_a, y_a)}{Z_j^H(\omega) Z_n(\omega)\gamma_j\gamma_n} \Big] A_{Q_j Q_n}(\omega) \tag{1}$$

where Ψ_j is the jth analytic mode shape, γ_j is the generalized mass coefficient for the same mode order, Z_j is the dynamic structural impedance and $A_{Q_j Q_n}$ is the well-known joint acceptance integral.

This approach, while giving a powerful tool for the validation of other numerical and experimental techniques, as in the present case, is valid in a limited set of cases. In fact, as described in [Elishakoff et al. (1983), De Rosa et al. (2008a), Franco et al. (2013), De Rosa et al. (2008b)], this analytic solution is developed and is easy to derive only for a flat, rectangular and simply-supported plate under a fully developed (ergodic) turbulent boundary layer modelled using the Corcos model [Corcos et al. (1963)]. The main complexity is, first, in the solution of the joint-acceptance integral and, then, in that the knowledge of the analytic formulation of structural modes is needed. The boundary layer induced vibrations are also analysed, in the literature, under different boundary conditions [Hambric et al. (2004)].

2.2 Modal solution for vibrations under random load

Within discretized FE framework, under the hypothesis of statistically stationary and ergodic random forces, the calculation of the displacement cross-spectrum matrix, $\mathbf{S}_{ww}$, can be performed as in Eq. 2 [Elishakoff et al. (1983)].

$$\mathbf{S}_{ww}(\omega) = \mathbf{\Psi}\mathbf{H}(\omega)\mathbf{\Psi}^T\mathbf{S}_{FF}(\omega)\mathbf{\Psi}\mathbf{H}^H(\omega)\mathbf{\Psi}^T \tag{2}$$

with

$$H_j(\omega) = \frac{1}{\omega_j^2 - \omega^2 + \mathrm{i}\eta\omega_j^2} \tag{3}$$

where $\mathbf{\Psi}$ is the matrix of the structural modes and $\mathbf{S}_{FF}$ is the load matrix in a FE framework. The elements of this matrix should be calculated with a surface integral on the nodal area of the product of the structural shape functions and the wall pressure cross spectra (WPS) [De Rosa et al. (2008b)]. However, considering that the pressure fluctuations, do not fluctuate very quickly in the nodal area, given by $\Delta_x\Delta_y$, a direct lump-on-the-nodes of the wall pressure cross spectra is a good approximation of the integral hidden in $\mathbf{S}_{FF}$, as in Eq. 4 [De Rosa et al. (2008a), Franco et al. (2013), De Rosa et al. (2008b)].

$$S_{FF_L}^{i,j} = X_{pp}(\xi_x^{ij}, \xi_y^{ij}, \omega)\Delta_x^2\Delta_y^2 \tag{4}$$

Eq. 4 is valid if the nodal area so small that the pressure is not fluctuating much in the considered spatial domain. This means that, once a mesh is fixed, Eq. 4 will be valid just up to a certain frequency, called aliasing frequency.

Within this work, the the coherence model for the wall pressure fluctuations proposed by Corcos et al. (1963), as in Eq. 5 and 6, is used.

$$\mathbf{X}_{pp}(\xi,\omega) = \mathbf{S}_p(\omega)\mathbf{\Gamma}(\xi_x,\xi_y,\omega) \tag{5}$$

where

$$\mathbf{\Gamma}(\xi_x,\xi_y,\omega) = \mathrm{e}^{-\alpha_x|\omega\xi_x/U_c|}\mathrm{e}^{-\alpha_y|\omega\xi_y/U_c|}\mathrm{e}^{\mathrm{i}|\omega\xi_x/U_c|} \tag{6}$$

U_c is the convective flow speed, $\mathbf{S}_p$ is the single-point auto spectral density of the wall pressure distribution, α_x and α_y are the correlation coefficients and ξ_x and ξ_y are the relative distances for the stream-wise and cross-wise directions respectively [Corcos et al. (1963)].

3. The Numerical Methodology

3.1 A Transfer Matrix Approach

Here a transfer matrix between the excited degrees of freedom and the target ones is used. Assuming a quantity of interest v, which can be representative of displacements, velocities, accelerations or pressures, the cross spectral densities among two points i and j to a random distributed pressure can be calculated as in Eq. 7.

$$S_{vv}(x_i,x_j,\omega) = \mathbf{L}_v^T(x_i,\omega)\mathbf{S}_{FF}(\omega)\mathbf{L}_v(x_j,\omega) \tag{7}$$

where $\mathbf{L}_v$ is the transfer matrix that links the target degrees of freedom (TDof) and the excited ones (EDof) and S_{vv} is the matrix of the auto/cross spectral densities. If, on the contrary, the excitation is distributed but deterministic, Eq. 8 can be used instead.

$$V(x_i,\omega) = \mathbf{L}_v^T(x_i,\omega)\mathbf{P}_F(\omega) \tag{8}$$

where V is the target quantity of interest, while $\mathbf{P}_F$ is the matrix describing the pressure load distribution. The first advantage of this approach relies in choosing the value of TDof depending on the analysis needs. This is particularly suitable if the target is represented by the vibrational levels on a localised part of the whole assembly (i.e. a junction). An extensive discussion of the advantages of the proposed method has been proposed by Errico et al. (2018b).

The elements of the transfer matrix represent transfer Green function between two points i and j. In this paper, the input Green functions are calculated through a wave-based technique and a reciprocity approach [Errico et al. (2018b)].

3.2 The Wave Finite Element Method (WFEM)

The adopted wave-based technique is a wave finite element (WFE) method applicable for homogeneous and periodic structures. The method makes use of the periodic conditions to move in the wavemode-basis, in which the problem is analysed through the superposition of

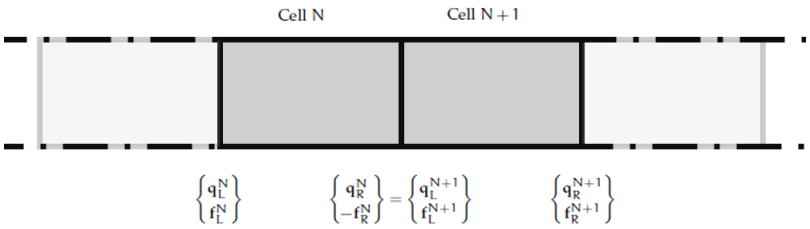

Fig. 1 Two adjacent elementary cells of a waveguide

different wavefields, [Brillouin et al. (1953), Mead et al. (1996), Manconi et al. (2008), Waki et al. (2009), Errico et al. (2018a)].

Considering a repetitive substructure of a periodic assembly, the Bloch-Floquet conditions (periodicity) can be easily applied considering a complex propagation constant linking the wavefields in the substructures' different points. For a single periodic system (in a 1-D formulation), the periodicity conditions become the equilibrium of the displacement and forces among the common hypernodes of two subsequent periodic cells (Fig. 1). In the following dynamic stiffness equations, the left and right side hypernodes are defined with the letters L and R respectively.

$$\begin{bmatrix} \mathbf{D}_{LL} & \mathbf{D}_{LR} \\ \mathbf{D}_{RL} & \mathbf{D}_{RR} \end{bmatrix} \begin{Bmatrix} \mathbf{q}_L \\ \mathbf{q}_R \end{Bmatrix} = \begin{Bmatrix} \mathbf{F}_L \\ \mathbf{F}_R \end{Bmatrix} \tag{9}$$

where $\mathbf{D}$ = [$\mathbf{K}$ - ω^2 $\mathbf{M}$]. For unit-cells involving complex cross-sections, a state vector reduction can be used to reduce the computational effort [Droz et al. (2014)]. It can be combined with Craig-Bampton (CB) dynamic condensation method of the inner degrees of freedom in case of structural periodicity [Droz et al. (2016)]

With simple substitutions in Eq. 9, one can get the so-called Transfer matrix, $\mathbf{T}$ that links nodal displacements and forces in two adjacent substructures [Manconi et al. (2008), Waki et al. (2009), Mencik et al. (2007), Mencik (2010)].

$$\left[\mathbf{T}\right] = \begin{bmatrix} -\mathbf{D}_{LR}^{-1}\mathbf{D}_{LL} & \mathbf{D}_{LR}^{-1} \\ -\mathbf{D}_{RL} + \mathbf{D}_{RR}\mathbf{D}_{LR}^{-1}\mathbf{D}_{LL} & -\mathbf{D}_{RR}\mathbf{D}_{LR}^{-1} \end{bmatrix} \tag{10}$$

Useful discussions on the properties of this matrix and the associated numerical issues, are present in the literature [Renno et al. (2014, 2013)]. In a wavemode-basis, the displacements and forces in the substructure section can be expressed as such:

$$\begin{Bmatrix} \mathbf{q}_L \\ \mathbf{f}_L \end{Bmatrix} = \begin{bmatrix} \mathbf{\Phi}_q^+ & \mathbf{\Phi}_q^- \\ \mathbf{\Phi}_f^+ & \mathbf{\Phi}_f^- \end{bmatrix} \begin{Bmatrix} \mathbf{a}^+ \\ \mathbf{a}^- \end{Bmatrix} \tag{11}$$

where $\mathbf{a}^{+,-}$ are the wave amplitudes of the positive and negative going waves. On the contrary, $\mathbf{\Phi}_q^{+,-}$ and $\mathbf{\Phi}_f^{+,-}$, represent specific partitions of the eigenvectors of the transfer matrix (Eq. 10) connected to the displacements and forces distributions is the waveguide section

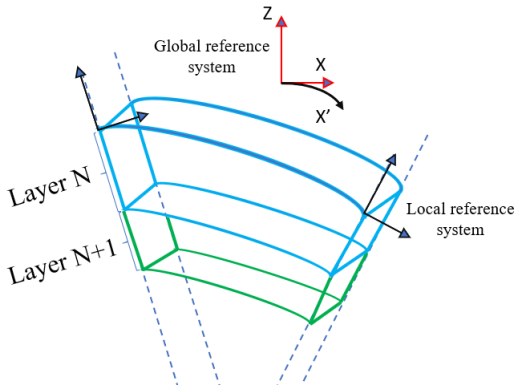

Fig. 2 The rotation of the global reference into the local one in each location and layer of the cell.

[Mead et al. (1996), Renno et al. (2014), Errico et al. (2018b)]. The filtering issues associated with the wave basis are deeply investigated in literature [Manconi et al. (2008), Mencik et al. (2007)] and are not repeated here. Moreover, the possibility of introducing variable meshes, within this framework, has been recently investigated by Errico et al. (2018b).

3.3 Forced Vibrations for Axisymmetric Structures

In a WFE framework, the forced vibrations can be evaluated through the superposition of the direct and reverberant field. The first is the result of the excitation and the second is the reverberant wavefield.

It is worth to highlight that the distributed rand excitation is not translated to the substructures' scale but is accounted using Eq. (7). The wave finite element method is here used to evaluate the transfer functions that compose the transfer matrix, using single input (single point) responses between the target and loaded degrees of freedom. Here, a general formulation to deal with axisymmetric and curved structures, even in presence of structural impedence variations along the periodicity direction and tapering, is presented. In fact, the main issue of the standard WFE formulation stands in the fact that the consecutive sub-domains can not be different from the previous one, whereas, for curved and tapered structures each point behaves on a circumference of different radius moving along the rotation axis.

First, the curvature of the substructure must be simulated rotating the degrees of freedom, as shown in Fig. 2. The idea is to rotate the local reference for each node belonging to the cell FE. In this way, imposing the periodicity conditions, as shown in Eq. 10, the wave propagation is automatically analysed along the imposed curved path. Moreover, a single FE model of the cell can be used to simulate different curvatures, and, apart from large periods, the cell can be modelled as totally flat.

A rotational matrix is assembled in a block diagonal matrix **Rot**, for each curvature. As in Fig. 2, the curvature simulation must be made for every layer composing the elementary cell. Each layer can have a different nature and even fluid-structure coupling at cell scale can be included if fluid layers are present [Manconi et al. (2009)].

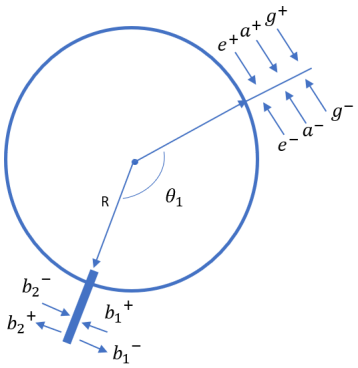

Fig. 3 Waves in an axial-symmetric jointed structure excited by a point load

The new mass and stiffness matrices of the curved cell can be calculated with a simple matrix product:

$$\begin{aligned} \mathbf{M} &= \mathbf{Rot}_j^T \mathbf{M}_{flat} \mathbf{Rot}_j \\ \mathbf{K} &= \mathbf{Rot}_j^T \mathbf{K}_{flat} \mathbf{Rot}_j. \end{aligned} \tag{12}$$

The waves, resulting from the eigenvalue problem of the transfer matrix (Eq. 10) represent circumferential waves and the angular distance between points (Eq. 13) can be used as a new reference. This approach can be particularly useful for tapered structures.

$$\boldsymbol{\lambda}_\theta = e^{-\mathbf{i}\mathbf{k}_\theta \Delta\theta} \tag{13}$$

where k_θ=$k_x R$=$k_x \Delta_x / \Delta\theta$ is the circumferential wavenumber, $\Delta\theta$ is the angular distance and R is the section radius (Fig. 3).

Using the wavemode-basis, the structural response can be calculated considering the superposition of an equivalent direct field and the reverberant one. When a closed axisymmetric structure is considered, the formulation presented by Errico et al. (2018b) can be used. Here, a more general formulation is presented to deal with joints and impedance variations along the circumference, as illustrated in Fig.3.

In the case some discontinuities, such as linear or complex joints, are reached by the waves, the scattering properties become largely impactive on the structural behaviour. Considering a junction as in Fig. 3 one can analyse the scattering properties taking into account the waves in the first and second waveguide, in terms of incident and outgoing (reflected and transmitted) wave amplitudes along the junction itself [Mitrou et al. (2017), Groby et al. (2009)]. In Fig. 3 this is illustrated with $\mathbf{b}_1^{-,+}$ and $\mathbf{b}_2^{-,+}$, at the edges of the structure. The scattering matrix $\mathbf{s}$ can be defined taking into account what just said and thus has the following expression:

$$\begin{Bmatrix} \mathbf{b}_1^- \\ \mathbf{b}_2^+ \end{Bmatrix} = \begin{bmatrix} \mathbf{s}_1 & \mathbf{s}_2 \\ \mathbf{s}_3 & \mathbf{s}_4 \end{bmatrix} \begin{Bmatrix} \mathbf{b}_1^+ \\ \mathbf{b}_2^- \end{Bmatrix} \tag{14}$$

where the scattering matrix has been splinted in four sub-matrices: $\mathbf{s}_1$ and $\mathbf{s}_4$ represent transmission matrices, while $\mathbf{s}_2$ and $\mathbf{s}_3$ represent reflection ones. The joint is assumed to be infinite in the direction normal to the propagation one and is modelled using finite elements. This assumption does not affect the results even for finite-size structures. It is to be underlined that there is no restriction on the type of FE model to be used for the joint.

Condensing the FE of the junction to the borders and express the dynamic equation of the junction as condensed to its edges, one gets Eq. 15. Typical methods are static condensations or a component mode synthesis [Droz et al. (2014)]. If internal forces are present, these can be substituted by structurally equivalent forces at the joint interface.

$$\mathbf{D}_J\ \mathbf{Q}_J = \ \mathbf{F}_J \tag{15}$$

where $\mathbf{Q}_J$ and $\mathbf{F}_J$ are the vectors of dofs and nodal forces of the joint to its borders.

Since the force and displacement vectors at the borders of the joint are in common with the two waveguides, they can be expressed in wave base using the wavemodes of each periodic substructure. Imposing the continuity and equilibrium conditions for the joint and using the eigenvectors of the two waveguides incident on the joint, the displacements $\mathbf{Q}_J$ and the force field $\mathbf{F}_J$ can be expressed in a wave-basis:

$$\mathbf{Q}_J = \begin{bmatrix} \Phi_q^{1,+}\mathbf{b}_1^+ + \Phi_q^{1,-}\mathbf{b}_1^- \\ \Phi_q^{2,+}\mathbf{b}_2^+ + \Phi_q^{2,-}\mathbf{b}_2^- \end{bmatrix} \tag{16}$$

$$\mathbf{F}_J = \begin{bmatrix} \Phi_f^{1,+}\mathbf{b}_1^+ + \Phi_f^{1,-}\mathbf{b}_1^- \\ -\Phi_f^{2,+}\mathbf{b}_2^+ - \Phi_f^{2,-}\mathbf{b}_2^- \end{bmatrix}. \tag{17}$$

Substituting the previous equations in the equilibrium equation of the joint (Eq. 15), condensed to boundaries, the scattering matrix can be obtained straightforwardly, as in Eq. 18.

$$\mathbf{s} = \left[-\mathbf{D}_J \begin{bmatrix} \Phi_q^{1,-} & \mathbf{0} \\ \mathbf{0} & \Phi_q^{2,+} \end{bmatrix} + \begin{bmatrix} \Phi_f^{1,-} & \mathbf{0} \\ \mathbf{0} & -\Phi_f^{2,+} \end{bmatrix} \right]^{-1} \left[\mathbf{D}_J \begin{bmatrix} \Phi_q^{1,+} & \mathbf{0} \\ \mathbf{0} & \Phi_q^{2,-} \end{bmatrix} - \begin{bmatrix} \Phi_f^{1,+} & \mathbf{0} \\ \mathbf{0} & -\Phi_f^{2,-} \end{bmatrix} \right] \tag{18}$$

The inversion in Eq. 18 can cause numerical instabilities and the use of the left eigenvalues is required [Mitrou et al. (2017)]. It should be underlined that the actual description is applicable also for lap joints, L-shaped, T-shaped or more complex junctions, as deeply investigated in [Renno et al. (2013), Mitrou et al. (2017)].

Once the amplitudes of direct wavefield are known, the amplitudes of the waves can be calculated at a given response point by considering the excitation, reflection and propagation relations. First the scattering equation can be solved obtaining the values of the incoming and out-coming waves at the joint:

$$b_2^+ = \left[\mathbf{I} - \mathbf{Tr}(2\pi - \theta_1)\mathbf{s}_4\mathbf{Tr}(2\pi - \theta_1)\right]^{-1}\left[\mathbf{Tr}(2\pi - \theta_1)\mathbf{s}_3\mathbf{Tr}(\theta_1)\right]a^+ \tag{19}$$

$$b_1^- = \mathbf{Tr}(\theta_1)\mathbf{s}_1\mathbf{Tr}(\theta_1)a^+ + \mathbf{Tr}(\theta_1)\mathbf{s}_2\mathbf{Tr}(\theta_1)b_2^+ \tag{20}$$

with θ_1 is the angular distance between the joint and the reference point chosen.

Using again Fig. 3 as reference, the amplitude of waves in the reference point can be calculated. The response in a target point can be finally expressed as:

$$\begin{aligned} a^+ = \big[\mathbf{I} - \mathbf{Tr}(2\pi-\theta_1)\mathbf{s}_3\mathbf{Tr}(\theta_1) - \mathbf{Tr}(2\pi-\theta_1)\mathbf{s}_4\mathbf{Tr}(2\pi-\theta_1)\big[\mathbf{I} - \mathbf{Tr}(\theta_1)\mathbf{s}_2\mathbf{Tr}(\theta_1)\big]^{-1} \\ \mathbf{Tr}(\theta_1)\mathbf{s}_2\mathbf{Tr}(\theta_1)\big]^{-1}\big[e^+ + \mathbf{Tr}(2\pi-\theta_1)\mathbf{s}_4\mathbf{Tr}(2\pi-\theta_1)\big[\mathbf{I} - \mathbf{Tr}(\theta_1)\mathbf{s}_2\mathbf{Tr}(\theta_1)\big]^{-1}e^-\big] \end{aligned} \tag{21}$$

$$a^- = \big[\mathbf{I} - \mathbf{Tr}(\theta_1)\mathbf{s}_2\mathbf{Tr}(\theta_1)\big]^{-1}\big[e^- + \mathbf{Tr}(\theta_1)\mathbf{s}_1\mathbf{Tr}(\theta_1)a^+\big] - e^- \tag{22}$$

Eqs. (21) and (22) represent the general solution when an impedance variation is also present on the circumferential wave-path. In the case the axisymmetric structure is homogeneous, or simply there is no variation of impedance, Eq. (21) and (22) remain the same, while the values of the $\mathbf{s}_J$ (J =1,. . . ,4) matrices change in zeros and identity matrices since a full transmission must be simulated.

In general, the structures might not be fully periodic. It might happen, however, that the entire structure can be identified as the sum of periodic parts connected through joints. In these cases, the technique presented above can still be considered valid if the scattering around the joint is taken into account. It is worth to highlight that the present formulations are more general than the ones proposed in Errico et al. (2018a, b).

4. Validating Results

4.1 Distributed Deterministic Pressure Loading

Here the structural vibrations of a cylindrical model are firstly validated and then investigated for different structural models, under an assigned pressure distribution. This pressure field is a simplified representation of the one induced by a rotating propeller on a cylindrical model of a fuselage. The pressure distribution is representative of a 100 Hz tonal harmonic load and a simple illustration is present in Fig. 4.

Both the global FE model and the substructure, are shown in Fig. 5. The cylindrical model is 9.7 m long and the diameter is 3.4 m. Free boundary conditions are imposed at the borders. The analysis is performed at 100 Hz and a validation with a full FEM calculation, in the case of a 2mm-thick aluminium shell, is shown in Fig. 6 for the whole set of points along the axis, belonging to two specific angular locations. In order to assure mesh convergence, a 10 elements per wavelength mesh has been used. The whole FE models has 48 elements in the circumferential direction and 43 in the axial one. The structure is modelled using ANSYS $SHELL181$ elements, in both cases. As observed in Fig. 6, the difference in percentage is limited under 0.2% along the whole set of points. While the classic FEM requires 12936 nodal DoFs, the WFE approach requires just 264 of them, reducing the size of the numerical problem by almost 98%.

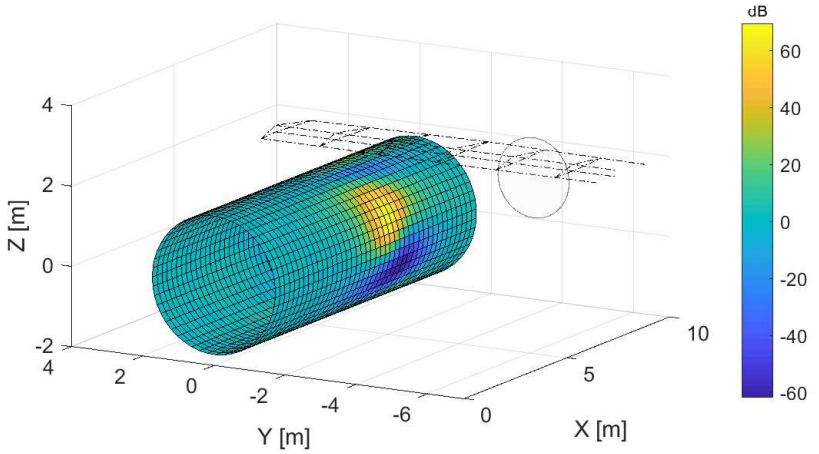

Fig. 4 Pressure distribution assumed on the cylindrical portion of a fuselage model at 100Hz, in Pa.

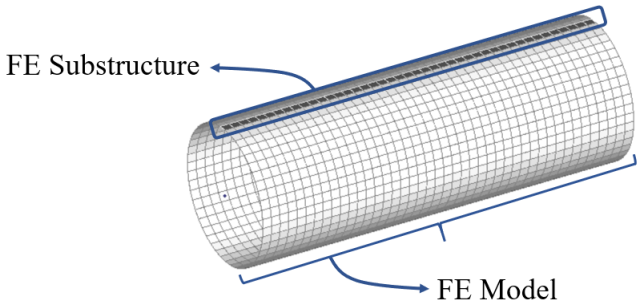

Fig. 5 The cylindrical structure used as a test-case: full finite element model and substructure in the framework of the proposed method.

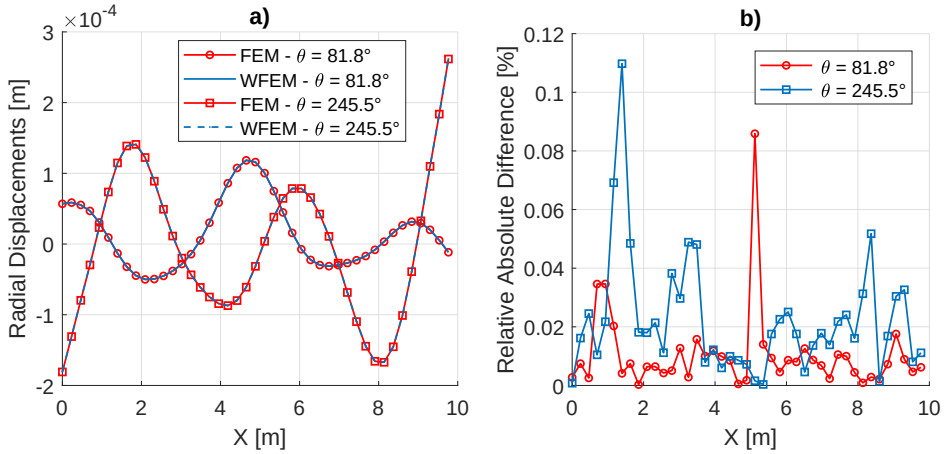

Fig. 6 A comparison between the proposed method and FEM. a) The radial displacements of the shell in two angular locations; b) The relative error in percentage.

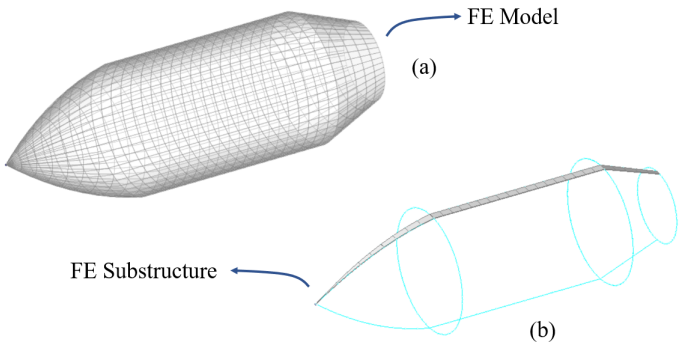

Fig. 7 A tapered axisymmetric structure, used as a test-case: full finite element model (a); substructure in the framework of the proposed method (b).

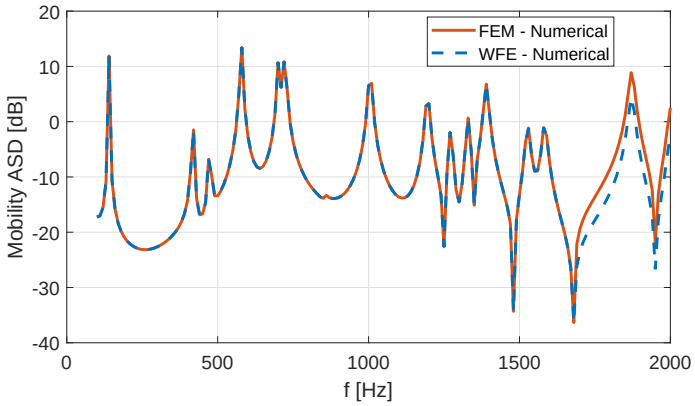

Fig. 8 Numerical results comparison for a fairing-like structure under diffuse acoustic excitation - Auto Spectral Density in one point, [dB ref. $(1\ \mathrm{m/s})^2/\mathrm{Hz}$].

4.2 Diffuse Acoustic Field

In this section, a complex and tapered axisymmetric structure, similar to a space launcher fairing (Fig. 7), is used as a test-case to prove the efficiency of the method and its flexibility. Due to gradient effects, it is not correct to apply a Corcos TBL model [Yang et al. (2017)]. An incident diffuse field (DAF) is simulated, instead, since it is often used to describe the TBL load in the low frequencies (i.e. load description on a space launcher fairing during take-off and climbing phases), overestimating the effects for increasing excitation frequency. In Fig. 7, the relative substructure used within the present approach is also shown. The structure is made again of aluminium. Fig. 8 shows the comparison between a full stochastic FE method and the proposed WFE with the TM approach. A computational cost comparison is also shown in Table 1; the reference FEM solution is calculated using a proper set of modes in Eq. (2), while the size of the load matrix in Eqs. (2), (7) and (4) is the same between the models. As expected, the two models are equivalent in terms of accuracy, up to the aliasing frequency, where the full stochastic finite element model starts to lose precision. The use

Table 1 Computational cost comparison for the sructural model in Fig. 7 under TBL load

Method	**Mesh Design Frequency** [kHz]	**Relative CPU Time/Frequency**	**Relative RAM Memory/Frequency**
FEM - Eqs.(2), (4)	2.0	43.8	5.8
WFE - Eq.(7), (4)	2.0	1.0	1.0

Table 2 Material Data of the Lamina

E_X [GPa]	E_Y [GPa]	$\rho[Kg/\mathbf{m}^3]$	G_{XY} [GPa]	G_{XZ} [GPa]	ν_{XY}
129	8.25	1600	4.23	4.23	0.0192

of the transfer matrix, in fact, strongly increases the flexibility in terms of selection of the degrees of freedom, both for the target and the wetted, while the wave-based method to evaluate the Green functions allows the use of a reduced model for all the calculation steps. In order to assure mesh convergence, a 10 elements per wavelength mesh has been used, and, again, the structure is modelled using ANSYS $SHELL181$ elements, in both cases.

5. Stacking Sequence Effects on the Structural Response

It is interesting now to compare different laminations for a composite laminate shell. In fact, a different stacking sequence can lead to a different wave propagation along the shell and thus a different vibration field for given excitation model. The set of configurations and stacking sequences analysed are listed in Table 2 and 3. Each lamina is 0.425mm thick and the laminate is composed by 8 layers, in each configurations. The 0° and 90° represent fibres orientations corresponding to the axial and circumferential directions of the cylinder. The choice of the sequences A and B, reported in Tab. 3, is justified by the need of having higher axial or circumferential bending stiffness, while the configurations C and D, apart from notching issues, that usually require ±45° orientations on the outside, is aiming to induce helical bending waves, attenuating the excitation of the purely circumferential and axial modes of the shell. Here a TBL excitation is again considered using a Corcos model. A simple application of this simple model to a cylindrical model is still acceptable, if the stream-wise direction is parallel to the axis of rotation and the cross-wise is assumed to be the circumferential one [Li et al. (2017)]. Of course, the model must be purely cylindrical (not tapered) to avoid pressure gradient effects which would invalidate the application of the Corcos model. The convective speed is 180 m/s. The cylindrical model analysed is 0.2m long and is 3.4mm thick. The auto spectral densities of the radial velocity are averaged in four random points and compared. A 10 elements per wavelength mesh has been used, and

Table 3 Stacking Sequences

A	**B**	**C**	**D**
$[90_2/0_4/90_2]$	$[0_2/90_4/0_2]$	$[\pm 45/0_4/\pm 45]$	$[\pm 45/90_4/\pm 45]$

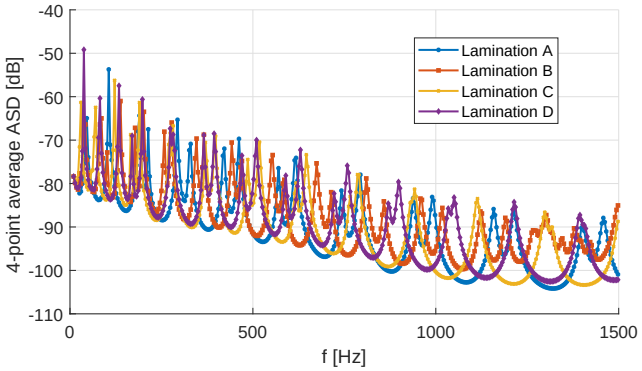

Fig. 9 Numerical results comparison. Cylinder under TBL (Radius 0.36m) - Auto Spectral Density averaged on four points, [dB ref. $(1\ \mathrm{m/s})^2/\mathrm{Hz}$].

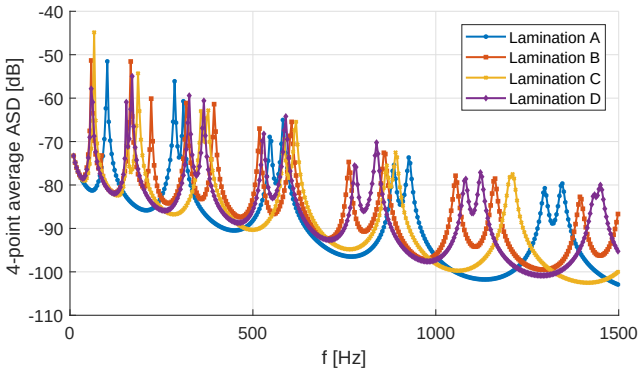

Fig. 10 Numerical results comparison. Cylinder under TBL (Radius 0.20m) - Auto Spectral Density averaged on four points, [dB ref. $(1\ \mathrm{m/s})^2/\mathrm{Hz}$].

the structure is modelled using ANSYS $SHELL181$ elements. Different cylinder radius are analysed: 0.36m in Fig.9, 0.2m in Fig.10, 0.12m in Fig.11. The results show that altering the lamination sequence the structural modes shift in frequency. However, having kept the mass of the structure constant (each lamina has the same density), the dynamic content in frequency is similar among the cases. In fact Fig. 9 shows how, for the configurations analysed, not much difference is observed. On the other hand, when the radius of the cylinder is reduced, as in Fig. 11, it is clearer how the best result is achieved with the configuration A, which is the stiffest in the stream-wise direction.

6. Conclusions

This work shows a numerical wave-based approach for the analysis of the vibrations of shell structures when convective loads are considered. The approach couples the translated load to the target degrees of freedom using numerical Green functions. A wave finite element method is reformulated in the case of curved and axisymmetric structures to cope

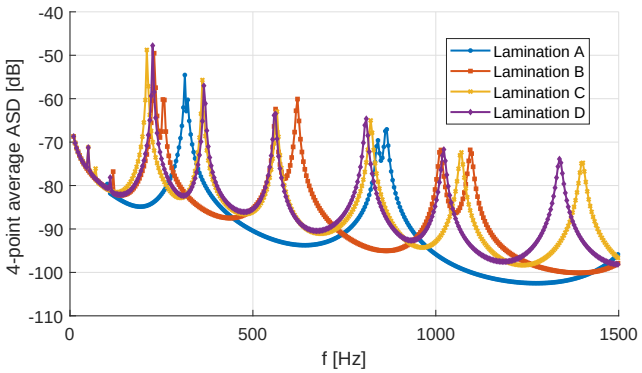

Fig. 11 Numerical results comparison. Cylinder under TBL (Radius 0.12m) - Auto Spectral Density averaged on four points, [dB ref. $(1\ \mathrm{m/s})^2/\mathrm{Hz}$].

with complex and tapered shapes. A dynamic or static condensation is also possible for complex cross-sectional geometries and the presence of joints or impedence variations along the circumference can also be modelled.

The analytical formulations are available for simple test-cases, while the classic FEM approaches can only cope with the lowest frequency ranges, due to computational cost issues, the present method aims to extend of the FE-based numerical analysis to higher frequencies within the medium frequency range, for a given computational cost, or a reduced calculation time, given a frequency band. The flexibility of the link between the structural and fluid mesh, gives the possibility of using a single substructure to analyse different test-cases.

The effects of the stacking sequence has been investigated with four different configurations, for three different length on radius ratios, showing how the stiffer the final laminate is in the stream-wise direction, the most attenuated the response is.

Acknowledgements

This project has received funding from the European Unions Horizon 2020 research and innovation program under the Marie Sklodowska-Curie grant agreement No. 675441. The author would like to gratefully acknowledge everyone involved in the VIPER project.

References

Bhat, W.V. (1971), Use of correlation technique for estimating in-ight noise radiated by wing-mounted jet engines on a fuselage, *J. Sound Vib.*, **17**(3), 349-355. https://doi.org/10.1016/0022-460X(71)90647-X.

Birgersson, F., Finnveden, S. and Robert, G. (2004), Modelling turbulence-induced vibration of pipes with a spectral finite element method, *J. Sound Vib.*, **278**(3), 749-772. https://doi.org/10.1016/j.jsv.2003.10.024..

Brillouin, L. (1953), *Wave Propagation in Periodic Structures: Electric Filters and Crystal Lattices*, 2nd Edition, Dover Publications, INC., Mineola, New York, U.S.A.

Chase, D.M. (1980), Modelling the wavevector-frequency spectrum of turbulent boundary layer wall pressure, *J. Sound Vib.*, **70**(1), 29-67. https://doi.org/10.1016/0022-460X(80)90553-2.

Christen, J.L., Ichchou, M., Zine, A. and Troclet, B. (2016), Wave finite element formulation of the acoustic transmission through complex infinite plates, *Acta Acust. United Acust.*, **102**(6), 984-991. https://doi.org/10.3813/AAA.919013.

Chronopoulos, D. (2012), Prediction of the vibroacoustic response of aerospace composite structures in a broadband frequency range, Ph.D. Thesis, Ecole Centrale de Lyon, Lyon, France.

E. Ciappi, F. Magionesi, S. De Rosa, F.Franco,(2012), "Analysis of the scaling laws for the turbulence driven panel responses",*J. Fluids Struct.*, **32**, 90-103. https://doi.org/10.1016/j.jfluidstructs.2011.11.003.

Corcos, G.M. (1963), Resolution of pressure in turbulence, *J. Acoust. Soc. Amer.*, **35**(2), 192-199. https://doi.org/10.1121/1.1918431.

DAlessandro, V. (2014), Investigation and assessment of the wave and finite element method for structural waveguides, Ph.D. Thesis, University of Naples Federico II, Naples, Italy.

De Rosa, S. and Franco, F. (2008a), Exact and numerical responses of a plate under a turbulent boundary layer excitation, *J. Fluids Struct.*, **24**(2), 212-230. https://doi.org/10.1016/j.jfluidstructs.2007.07.007.

De Rosa, S. and Franco, F. (2008b), A scaling procedure for the response of an isolated system with high modal overlap factor, *Mech. Syst. Signal Process.*, **22**(7), 1549-1565. https://doi.org/10.1016/j.ymssp.2008.01.007.

Droz, C., Zhou, C., Ichchou, M.N. and Laine, J.P. (2016), A hybrid wave-mode formulation for the vibro- acoustic analysis of 2D periodic structures, *J. Sound Vib.*, **363**, 285-302. https://doi.org/10.1016/j.jsv.2015.11.003.

Droz, C., Laine, J.P., Ichchou, M. and Inquiete, G. (2014), A reduced formulation for the free-wave propagation analysis in composite structures, *Compos. Struct.*, **113** 134–144. https://doi.org/10.1016/j.compstruct.2014.03.017.

I. Elishakoff,(1983), *Probabilistic Method in Theory of Structures*, John Wiley and Sons, New York, U.S.A.

Emtsov, B.M. (1982), Characteristics of the eld of turbulent wall pressure uctuations at large Reynolds numbers, *Soviet Phys. Acous.*, **28** (4), 289–292.

Errico, F., Ichchou, M.N., De Rosa, S., Bareille, O. and Franco, F. (2018a), A WFE and Hybrid FE/WFE technique for the forced response of stiffened cylinders, *Adv. Aircraft Spacecraft Sci.*, **5**(1), 1-19. https://doi.org/10.12989/aas.2018.5.1.001.

Errico, F., Ichchou, M.N., De Rosa, S., Bareille, O. and Franco, F. (2018b), The modelling of the flow-induced vibrations of periodic at and axial-symmetric structures with a wave-based method, *J. Sound Vib.*, **424** 32–47. https://doi.org/10.1016/j.jsv.2018.03.012.

Franco, F., De Rosa, S. and Ciappi, E. (2013), Numerical approximations on the predictive responses of plates under stochastic and convective loads, *J. Fluids Struct.*, **42**, 296-312. https://doi.org/10.1016/j.jfluidstructs.2013.06.006.

Groby, J.P., Wirgin, A., De Ryck, L., Lauriks, W., Gilbert, R.P. and Xu, Y.S. (2009), Acoustic response of a rigid-frame porous medium plate with a periodic set of inclusions,*J. Acoust. Soc. Am.*, **126**(2), 685-693. https://doi.org/10.1121/1.3158936.

Hambric, S.A., Hwang, Y.F. and Bonness, W.K. (2004), Vibration of plates with clamped and free edges excited by low-speed turbulent boundary layer,*J. Fluids Struct.*, **19** 93-110. https://doi.org/10.1016/j.jfluidstructs.2003.09.002.

Ichchou, M.N., Hiverniau, B. and Troclet, B. (2009), Equivalent rain on the roof loads for random spatially correlated excitations in the mid frequency range, *J. Sound Vib.*, **322**, 926-940. https://doi.org/10.1016/j.jsv.2008.11.050.

Kolaini, A.R., Tsuha, W. and Fernandez, J.P. (2018), Spacecraft vibration testing: Benefits and potential issues, *Adv. Aircraft Spacecraft Sci.*, **5**(2), 165-175. https://doi.org/10.12989/aas.2018.5.2.165.

Li, Y., Zhang, Y. and Kennedy, D. (2017), Random vibration analysis of axially compressed cylindrical shells under turbulent boundary layer in a symplectic system, *J. Sound Vib.*, **406**, 161-180. https://doi.org/10.1016/j.jsv.2017.06.018.

Lyon, R.H. and DeJong, G. (1995), *Theory and application of Statistical Energy Analysis*, Buttersworths-Heimann.

Manconi, E. and Mace, B.R. (2008), Modelling wave propagation in two dimensional structures using finite element analysis, *J. Sound Vib.*, **318**(45), 884-902. https://doi.org/10.1016/j.jsv.2008.04.039.

Manconi, E. and Mace, B.R. and Garziera, R. (2009), Wave finite element analysis of uid-ıledpipes, *Proceedings of the NOVEM 2009 Conference.*

Mead, D.J. (1996), Wave propagation in continuous periodic structures: research contributions from Southampton, 1964-1995, *J. Sound Vib.*, **190**(3), 495-524. https://doi.org/10.1006/jsvi.1996.0076.

Mehta, R.C. (2017), Analysis of payload compartment venting of satellite launch vehicle, Adv. Aircraft Spacecraft Sci., **4**(4), 437448. https://doi.org/10.12989/aas.2017.4.4.437.

Mencik, J.M. and Ichchou, M.N. (2007), Wave finite elements in guided elastodynamics with internal fluid, *Int. J. Solids Struct.*, **44**, 2148-2167. https://doi.org/10.1016/j.ijsolstr.2006.06.048.

Mencik, J.M. (2010), On the low- and mid-frequency forced response of elastic structures using wave finite elements with one-dimensional propagation, *Comput. Struct.*, **88**, 674-689. https://doi.org/10.1016/j.compstruc.2010.02.006.

Mitrou, G., Ferguson, N. and Renno, J. (2017), Wave transmission through two-dimensional structures by the hybrid FE/WFE approach, *J. Sound Vib.*, **389** 484-501. https://doi.org/10.1016/j.jsv.2016.09.032.

Morsbl, J. and Sorokin, S.V. (2015), Elastic wave propagation in curved exible pipes, *Int. J. Solids Struct.*, **75**, 143-155. https://doi.org/10.1016/j.ijsolstr.2015.08.009.

J. M. Renno, B.R. Mace,(2014), Calculating the forced response of cylinders using the wave and finite element method, Journal of Sound and Vibration **333**, 5340–5355

Renno, J.M. and Mace, B.R. (2014), Calculating the forced response of cylinders using the wave and finite element method, *J. Sound Vib.*, **332**(21), 2149-2164. https://doi.org/10.1016/j.jsv.2014.04.042.

Renno, J.M. and Mace, B.R. (2014), Vibration modelling of structural networks using a hybrid finite element/wave and finite element approach, *Wave Motion*, **51** (4), 566-580. https://doi.org/10.1016/j.wavemoti.2013.09.001.

Smolyakov, A.V. and Tkachenko, V.M. (1991), Model of pseudosonic turbulent wall pressures and experimental data, *Soviet Phys. Acous.*, **37**(6), 627-631.

Troclet, B., Hiverniau, B., Ichchou, M.N., Jezequel, L., Kayvantash, K., Bekkour, T., Mouillet, J.B. and Gallet, A. (2009), FEM/SEA hybrid method for predicting mid and high frequency structure-borne transmission, *Open Acoust. J.*, **2**, 45–60. http://dx.doi.org/10.2174/1874837600902010045.

Vaquer-Araujo, X., Schottle, F., Kommer, A. and Konrad, W. (2018), Static and dynamic load superposition in spacecraft structural analysis, *Adv. Aircraft Spacecraft Sci.*, **5**(2), 259275. https://doi.org/10.12989/aas.2018.5.2.259.

Waki, Y., Mace, B.R. and Brennan, M.J. (2009), Numerical issues concerning the wave and finite element method for free and forced vibrations of waveguides, *J. Sound Vib.*, **327**, 92-108. https://doi.org/10.1016/j.jsv.2009.06.005.

Wilby, J.F. and Gloyna, F.L. (1972), Vibration measurements of an airplane fuselage structure II. Jet noise excitation, *J. Sound Vib.*, **23**(4), 467-486. https://doi.org/10.1016/0022-460X(72)90504-4.

Williams, J.F. (1982), Boundary layer pressures and the Corcos model: a development to incorporate low wavenumber constraints,*J. Fluid Mech.*, **125**, 9-25. https://doi.org/10.1017/S0022112082003218.

Yang, M.Y., Palodichuk, M.T., Murray, N.E. and Jansen, B.J. (2017), Prediction of structural response in transonic flow using wavenumber decomposition of fluctuating pressures, *Proceedings of the 23rd AIAA/CEAS Aeroacoustics Conference*, Denver, Colorado, U.S.A., June.

CC